Geophys. J. Int. (1995) 123, 849–865

The singularity mystery associated with a radially continuous Maxwell viscoelastic structure

Ming Fang and Bradford H. Hager

Department of Earth, Atmospheric, and Planetary Sciences, Massachusetts Institute of Technology, Cambridge, MA 02139, USA

Accepted 1995 June 21. Received 1995 May 1; in original form 1994 December 8

SUMMARY

The singularity problem associated with a radially continuous Maxwell viscoelastic structure is investigated. A special tool called the isolation function is developed. Results calculated using the isolation function show that the discrete model assumption is no longer valid when the viscoelastic parameter becomes a continuous function of radius. Continuous variations in the upper mantle viscoelastic parameter are especially powerful in destroying the mode-like structures. The contribution to the load Love numbers of the singularities is sensitive to the convexity of the viscoelastic parameter models. The difference between the vertical response and the horizontal response found in layered viscoelastic parameter models remains with continuous models.

Key words: mantle viscosity, Maxwell rheology, modes, singularity.

1 INTRODUCTION

In his remarkable monograph 'Theory of Viscoelasticity, an Introduction' Christensen (1971) warned that the extension of methods developed for homogeneous materials to inhomogeneous materials may be difficult, if not impossible. He did not, however, detail how and when the difficulties would occur. Three years later, in studying the viscoelastic response of the mantle to deglaciation, Peltier (1974) published perhaps the first such extension for a Maxwell viscoelastic rheology. In his paper, Peltier (1974) assumed that, for an inhomogeneous viscoelastic parameter $\eta(r)/\mu(r)$, which is a piecewise continuous function of radius, r, the relaxation of the Maxwell mantle is in the form of a set of discrete exponentially decaying time functions $\exp(s_j t)$, $s_j < 0$, $j = 1, 2, 3, \cdots$ (modes). This assumption is warranted in an exact sense when $\eta(r)/\mu(r)$ is formed by homogeneous layers (e.g. Wu & Peltier 1982). Each viscosity jump introduces two 'viscosity' modes (see below) and each density jump causes one 'buoyancy' mode (Han & Wahr 1995). The secular equation for these modes can be written as

$$\sum_{n=0}^{2N+M} \alpha_n s^n = 0,$$

where N and M are the numbers of viscosity jumps and density jumps, respectively. If we follow the spirit of using more and more layers to approximate a continuous structure, we encounter a theoretical crisis at its limit, namely, the solution of the secular equation becomes meaningless when $2N + M$ tends to infinity. Practically, it is very difficult to derive analytic expressions for the coefficients α_n even for fairly small N, say $N = 10$. The solution of the resulting high-order algebraic equation is also a big problem. Hence, most people turn to the Runge–Kutta propagation technique, commonly called the normal mode method (in this paper, the term 'normal mode method' is only used in relation to the propagation technique), to search for the discrete modes (e.g. Wu and Peltier 1982; Peltier 1985; Han & Wahr 1995). In this way, the 'theoretical crisis' mentioned above shifts to a singularity problem.

To be specific, let

$$s_{\min} = \min\left[-\frac{\mu(r)}{\eta(r)}\right], \qquad s_{\max} = \max\left[-\frac{\mu(r)}{\eta(r)}\right].$$

Then, for a fixed Laplace transform variable $s < 0$ satisfying $s_{\min} \le s \le s_{\max}$, there is at least one r_0 at which the Laplace-transformed Lamé parameters for Maxwell rheology,

$$\lambda(s, r) = \frac{\lambda s + \mu\kappa/\eta}{s + \mu/\eta}, \qquad \mu(s, r) = \frac{\mu s}{s + \mu/\eta},$$

become singular. We will call the set of all r_0 a singular bound. For a model with N layers, there are only N points within the singular bound. We can prove (e.g. Fang, Hager & Herring, in preparation) that a mode can never be exactly at the singular value $s = -\mu/\eta$ except when two adjacent layers degenerate into a single uniform layer. However, as the number of layers increases to infinity, the singular bound tends to span the entire closed interval $[s_{\min}, s_{\max}]$, and we have trouble determining if there are modes within the singular bound. This situation is equivalent to the 'theoretical crisis' with the secular equation at $N \to \infty$. Following the spirit of using more and more layers to approximate a continuous function, we can interpret the singular bound $[s_{\min}, s_{\max}]$ as representing a continuous spectrum of modes (Han & Wahr 1995). Modes, as we call them, are indeed poles on the complex Laplace

transform plane. Poles must be isolated. A cluster point of an infinite number of poles is a non-isolated singularity (Colombo 1983). As poles tend to be continuous, every point becomes a cluster point, and thus a non-isolated singularity. This is an unusual situation even in the context of complex analysis of one variable. It is not the intent of this paper to establish a general treatment in mathematical theory of such 'continuous poles'. Rather, we will focus on how and to what extent the 'continuous poles' contribute to the relaxation process of a Maxwell earth. This brings about the key question: how can we investigate the 'continuous poles'?

There are two major obstacles associated with the normal mode method that have previously prevented us from making a detailed investigation of the 'continuous poles'. First, the normal mode method is designed on the assumption of isolated poles. In order to trap a mode, we need a small interval $[s_1, s_2]$. If the determinants of the boundary matrix $\mathbf{M}(s_1)$ and $\mathbf{M}(s_2)$ are of opposite signs, and $\mathbf{M}(s)$ is approximately a linear function in $[s_1, s_2]$, then there is a pole at s_0 ($s_1 \le s_0 \le s_2$) such that $\mathbf{M}(s_0) = 0$. This small interval is not only practically important, but also theoretically required as, again, a pole must be isolated such that there is a neighbourhood of s_0 in which no other poles exist. When poles become continuous, the distance between each adjacent pole tends to zero, and the basic assumption of isolated poles no longer applies. Even if we can find a way to circumvent the difficulty and manage to isolate the poles, the obstacle is still not removed. As discussed later on, since the number of poles is infinite, the residues of the poles must be zero, except for a finite number of them. However, 'continuous poles' as a whole may well have a non-zero contribution and may even form the entire contribution to the relaxation process (see Section 4 below). This problem reflects a fundamental difference between a discrete treatment and a continuous treatment.

Runge–Kutta propagation is a method of using discretized layers to approximate a continuous function. One may reasonably argue that we are practically dealing with discrete modes by using Runge–Kutta propagation while we are thinking of 'continuous modes'. This argument is only one side of the story. On the other hand, discretization is a process of sampling. By sampling, we lose resolution power. If the original structure has two modes quite close to one another, a discretization with poor resolution power will lump them together to form a 'continuous spectrum'. This is quite similar to the Nyquist sampling problem in the area of data processing. What is happening on real numerical groups is a trade-off between these two conflicting mechanisms. We can look at the problem in a slightly different way. A discretization introduces error to the solution of a continuous structure. It is the same source of error as for a layered structure. A good numerical algorithm should be able to identify the differences between a continuous structure and a layered structure above the error level. Below the error level, it is meaningless to talk about either a continuous structure or a layered structure. We assume, throughout this paper, that our numerical algorithm is 'good'. If this assumption were to be invalidated by actual calculations, we have to consider replacing the currently used Runge–Kutta propagation with some more accurate scheme—for instance, upgrading the Runge–Kutta scheme from fourth order to sixth order.

The second problem with the normal mode method is that it forces the propagation to cross the singularity radius r_0. The normal mode method used is an extension of the seismic normal mode technique (e.g. Takeuchi & Saito 1972). Starting from the centre of the Earth, numerical integration of the dynamic equations propagates upwards to the surface to meet the boundary conditions for a trial mode. There is never a problem with such propagation for an elastic earth model, but there is a problem for a Maxwell viscoelastic model in the Laplace transform domain; namely, the propagation breaks up at r_0 for a trial mode s within the singular bound. Forcing the numerical integration to go through r_0 results in a series of noisy singular solutions for the set of trial modes s within the singular bound (e.g. Wu & Peltier 1982). These noisy singular solutions have caused concern (e.g. Mitrovica & Peltier 1992; Fang & Hager 1994; Han & Wahr 1995). Han & Wahr (1995) introduced a 'zero crossing criterion' to remedy this situation. It helps to identify some prominent modes that would otherwise have been buried among the noisy singular solutions, but it does not avoid the appearance of such noisy singular solutions. Thus it is of little help in assessing the singular bound contributions. This problem is related to the first obstacle mentioned above, namely, that the power of a discrete pole method becomes diminished when dealing with 'continuous poles'.

For most practical problems, the Laplace transform is used to improve the convergence of transform integrals. For a Maxwell rheology, however, the convergence is not a problem at all, even for the ordinary Fourier transform. Fang & Hager (1994) realized that the singularities can be avoided by extending the ordinary Fourier transform into the complex frequency domain (equivalent to the Laplace transform in its original form) but the time inversion along this line is extremely difficult. Fang & Hager (1994) modified the inversion procedure, and called it the complex real Fourier transform (CRFT) method. A more straightforward method that avoids the singularities is proposed by Hanyk *et al.* (1995). This is a direct time-domain solution so that singularities appearing in the frequency domain no longer exist. Yet none of these 'lumped response' methods is able to provide direct answers concerning the roles that the singularities play in the relaxation process.

In the past 20 yr, extensive investigations have been carried out on the discrete modes caused by the seismically identified discontinuities such as the 670 km boundary, CMB, the lithosphere and so on. Luckily enough, for the simple layered viscosity models used in these investigations (e.g. Nakada & Lambeck 1989; Tushingham & Peltier 1991; Han & Wahr 1995), these prominent modes caused by the discontinuities are mainly located outside the singular bound. Furthermore, these prominent modes seem to dominate the time responses. This latter conclusion comes from the 'inviscid fluid criterion' proposed by Wu & Peltier (1982). The 'inviscid fluid criterion' concerns the final state of equilibrium with time $t \to \infty$. Consider two admissible respones $w(t)$ and $w_1(t)$:

$$w_1(t) = w(t) + e^{-\sigma t} \sum_{n=1} r_n(\sigma) t^n, \qquad \sigma > 0.$$

The σ term in $w_1(t)$ is a typical component for a second- or higher-order mode. The final states $w(\infty)$ and $w_1(\infty)$ are the same. In this sense, the inviscid fluid criterion is not unique and incomplete. Nevertheless, it does indicate that, for these specific layered viscosity models, the singular bound contribution does not extend to a sufficiently long time.

Studies of the creep mechanisms for silicates (e.g. Weertman 1978; Ranalli 1991) indicate that a 'realistic' viscosity structure is likely to be piecewise continuous, and a layered structure is 'unrealistic'. Could the general features revealed from studies of those 'unrealistic' models apply to the 'realistic models'? Could a continuous structure generate prominent discrete modes? Is there a possibility that a singular bound contribution dominates the time response? All these important questions among others are related to one, namely, what is the real picture behind the noisy singular solutions?

In this paper we try to give a thorough and unified account of the singularity contributions to the relaxation process. This goal is achieved by the introduction of what we call the 'isolation function' in the Laplace s plane. Using the isolation function, we are able to isolate the effect of each individual singularity, whether it is a simple pole, part of a 'continuous mode' spectrum, a branch point, or even essential singularities, etc. Because our treatment is fairly general, and no presumption is made of the nature of the singularities, we will follow the informal spirit to use the terms 'continuous poles' or 'continuous modes'. We start in Section 2 with the basic mathematical framework and an outline of some exact solutions needed for later analysis. Section 3 is devoted to the introduction of the isolation function. Then, in Section 4, we present the results of isolation functions for a number of admissible viscosity models. Also in this section, we investigate the contributions of the singular bounds to the total load Love numbers. Finally in Section 5, there is the conclusion. In the Appendix we give a procedure for dealing with the singularities in the search for discrete modes on the negative side of the real axis in the s plane. The key to the procedure is a power series solution of the basic equations expanded about a singularity point. We provide details of the solution.

2 EXACT MODE SOLUTIONS

2.1 Basic equations

We consider, throughout this paper, a non-rotating, spherically symmetric, self-gravitating, incompressible mantle with uniform density ρ_m and uniform shear modulus μ. The effect of an inviscid core is taken into account by the boundary conditions and density contrast $\Delta\rho_{CMB}$ at the core–mantle boundary (CMB). The only reason for choosing such a simplified earth model is that we have a closed analytical mode solution for layered rheological parameters, so that a direct check can be made for the main results obtained numerically. For an infinitesimal displacement field $\mathbf{u}$, we have the unified quasi-static governing equations in the Laplace transform s domain (e.g. Wolf 1994; Fang *et al.* in preparation):

$$-\nabla p_1 - \rho_m \nabla \phi_1 + \frac{dE}{dr}\left(2\frac{\partial \mathbf{u}}{\partial r} + \hat{\mathbf{r}} \times \nabla \times \mathbf{u}\right) - E\nabla \times \nabla \times \mathbf{u} = 0, \tag{1}$$

$$\nabla \cdot \mathbf{u} = 0, \tag{2}$$

$$\nabla^2 \phi_1 = 0, \tag{3}$$

where p_1 is the incremental reduced pressure, ϕ_1 is the incremental self-gravitational potential caused by the surface and CMB deflections, and

$$E = \begin{cases} \mu & \text{elastic solid,} \\ \eta s & \text{viscous fluid,} \\ \dfrac{\mu s}{\mu/\eta + s} & \text{viscoelastic body.} \end{cases}$$

Following the conventional treatment (e.g. Alterman, Jarosh & Pekeris 1959), we decompose $\mathbf{u}$, ϕ_1, and p_1 into harmonic expansions:

$$\mathbf{u} = \sum_{n=1}^{\infty}\left[\hat{\mathbf{r}} U_n(r, s)P_n(\cos\theta) + \hat{\boldsymbol{\theta}}\frac{\partial}{\partial\theta} V_n(r, s)P_n(\cos\theta)\right],$$

$$\phi_1 = \sum_{n=1}^{\infty} \Phi_n(r, s)P_n(\cos\theta),$$

$$p_1 = \sum_{n=1}^{\infty} \psi_n(r, s)P_n(\cos\theta),$$

where P_n represent the Legendre polynomials, and θ is the colatitude. The solution for (3) is straightforward:

$$\Phi_n = A_n(s)r^n + B_n(s)r^{-n-1},$$

where A_n and B_n are the integral constants to be determined. To solve for the rest of the unknowns, let us define the column vector

$$\mathbf{Y} = (U_n, -\psi_n + T_{rn} - \rho_m\Phi_n, V_n, T_{\theta n})^T \tag{4}$$

where T_{rn} and $T_{\theta n}$ are the normal and shear stress components, respectively, for harmonic degree n. Then, eqs (1) and (2) can be reduced to a set of ordinary differential equations for each harmonic degree n:

$$\frac{d\mathbf{Y}}{dr} = \mathbf{M}\mathbf{Y}, \tag{5}$$

where

$$\mathbf{M} = \begin{bmatrix} -\dfrac{2}{r} & 0 & \dfrac{n(n+1)}{r} & 0 \\ \dfrac{12E}{r^2} & 0 & \dfrac{6En(n+1)}{r^2} & \dfrac{n(n+1)}{r} \\ -\dfrac{1}{r} & 0 & \dfrac{1}{r} & \dfrac{1}{E} \\ -\dfrac{6E}{r^2} & -\dfrac{1}{r} & \dfrac{2E(2n^2+2n-1)}{r^2} & -\dfrac{3}{r} \end{bmatrix}.$$

For those E of complex value (e.g. Section 3), eq. (5) could be made double size:

$$\frac{d}{dr}\begin{bmatrix}\mathbf{Y}_R \\ \mathbf{Y}_I\end{bmatrix} = \begin{bmatrix}\mathbf{M}_R & -\mathbf{M}_I \\ \mathbf{M}_I & \mathbf{M}_R\end{bmatrix}\begin{bmatrix}\mathbf{Y}_R \\ \mathbf{Y}_I\end{bmatrix}, \tag{6}$$

where $\mathbf{Y}_R$, $\mathbf{M}_R$ and $\mathbf{Y}_I$, $\mathbf{M}_I$ are the real parts and imaginary parts of $\mathbf{Y}$ and $\mathbf{M}$, respectively.

Free-slip boundary conditions are imposed on both the surface and CMB (e.g. Richards & Hager 1984) for a pure relaxation process, while for the surface loading problem, additional loading terms introduced by Longman (1962) are added to the radial stress component of the surface boundary condition and the perturbed gravitational potential. Physical variables Y, Φ_n, and $\partial\Phi_n/\partial r$ are all continuous at viscosity discontinuities. The extension of the boundary conditions from real to complex is straightforward.

The viscous parts of the vertical and horizontal load Love numbers, $\tilde{h}_n$ and $\tilde{l}_n$, for a Maxwell rheology are defined following Peltier (1974) as

$$\tilde{h}_n = h_n - h_n^e, \qquad \tilde{l}_n = l_n - l_n^e, \tag{7}$$

where h_n, l_n are the total load Love numbers and h_n^e, l_n^e are their elastic counterparts. The third Love number, k_n, is strictly proportional to h_n for our earth model, and is therefore not considered. For simplicity, we also call $\tilde{h}_n$ and $\tilde{l}_n$ the Love numbers.

2.2 Two-layer solution

We outline and discuss the results. Details of how these results are obtained can be found in Fang *et al.* (in preparation). Consider a set of two-layer viscosity models with a uniform lithosphere of 120 km thickness and increased viscosity η_{lith} overlying a uniform mantle of a fixed viscosity η_m at the value of the so-called background viscosity, $\eta_0 = 10^{21}$ Pa s. Other necessary physical parameters are listed in Fig. 7. The time response of the Maxwell Love numbers to an impulse can be written as a sum of modes:

$$\begin{Bmatrix} \tilde{h}_n \\ \tilde{l}_n \end{Bmatrix} = \sum_{j=1}^{4} \begin{Bmatrix} {}_h r_j^n \\ {}_l r_j^n \end{Bmatrix} \exp(s_j t), \qquad s_j < 0, \tag{8}$$

where s_j is the eigenvalue of the jth mode. Two out of the four modes are caused by the density contrasts at the surface and CMB, and the other two are excited by the viscosity discontinuity at 120 km depth. Note that there are two discrete singularities for such two-layer viscosity models, namely

$$-\frac{1}{s_{\max}} = \frac{\eta_{\text{lith}}}{\mu}, \qquad -\frac{1}{s_{\min}} = \frac{\eta_m}{\mu}. \tag{9}$$

It is more convenient in this situation to use the notion of reciprocal singular bound defined as $[-1/s_{\min}, -1/s_{\max}]$, since $-1/s$ corresponds to the relaxation time. Fig. 1 shows relaxation time spectra for six viscosity models for both a viscous and a Maxwell rheology. We adopt the notation from Wu & Peltier (1982) of mantle modes (M) and core modes (C), while we call the third spectrum of modes, to which they gave the name lithosphere modes (L), the viscosity modes (V), because the horizontal eigenfunctions of these modes clearly show the viscosity contrast (Fang *et al.* in preparation). Our identification of modes is also different from Wu & Peltier (1982) in the C modes and V modes before 'transition degree' 6.

There is a fourth spectrum of modes which we name the surface modes (S). These modes have been practically neglected in previous studies but turn out to be very useful in our analysis. In fact, a Newtonian viscous fluid always has two groups of gravitational modes: the core modes (C) excited by the CMB, and the surface modes (S) generated by the surface boundary. For a uniform viscosity model, a Maxwell body also has only two spectra of modes, S and C (Fig. 1a). The overlapping M and V modes in Fig. 1(a) are zero amplitude modes, as there is no viscosity contrast there. Non-zero M and V modes occur when the viscosity contrast is not zero. Fig. 2 shows the relative strengths of the C, V, and M modes in the Love numbers for the viscosity model in Fig. 1(f). The strength function is defined by

$${}_h\gamma_j^n = \frac{-{}_h r_j^n/s_j}{\sum_{j=1}^{4} |{}_h r_j^n/s_j|}, \qquad {}_l\gamma_j^n = \frac{-{}_l r_j^n/s_j}{\sum_{j=1}^{4} |{}_l r_j^n/s_j|}, \qquad j = 1, 2, 3, 4.$$

This strength function is similar to that used by Wu & Peltier (1982). In their case, the signs of all the amplitudes of the vertical responses are consistent, so that there is no need to take special care of the denominator. Here we encounter a situation where the horizontal responses can have opposite signs (see below). A direct summation will result in cancellation of the magnitude at the denominator. We choose the absolute value of the amplitude of each mode to form the denominator. The meaning of the strength function in this case is different from that used by Wu & Peltier (1982).

As seen in Fig. 2, for models with a lithosphere thickness of 120 km, the total strength of a Love number is mainly shared by the three M, C, and V modes. The contribution from the S modes is negligible. This is why the S modes have always been ignored in previous studies. However, this is not always true for different lithospheric models. If we (artificially) increase the thickness of the lithosphere to 1000 km, the picture of the strength function is quite different (see Fig. 3).

Two important observations can be made concerning Figs 1, 2 and 3. First, the eigenvalues s_j of the two modes excited by the viscosity contrast are very close to each other when the viscosity contrast is small. It is reasonable to extrapolate that, as $s_{\min} \to s_{\max}$, the gap between the two modes excited by the viscosity contrast will tend to zero. Additional numerical tests support this extrapolation and we do not see how it could happen otherwise. This observation implies both the existence of 'continuous modes' for a continuous viscosity and the association of the singular bound with the 'continuous modes'. Note that a viscosity contrast corresponds to two discrete singularities (see eq. 9), and a viscosity contrast creates two modes. Therefore, we can say that one singularity claims one mode, or equivalently, the number of the V modes and M modes is equal to the number of singularities. This singularity-mode-correspondence feature extends to layered models of any number of layers (Fang *et al.* in preparation).

Secondly, if we fix the thickness of the lithosphere at 120 km and increase the viscosity contrast, or, equivalently, increase the reciprocal singular bound, more modes will be trapped into the reciprocal singular bound. Fig. 2 shows that, for sufficiently high viscosity contrasts (larger than a factor of 20), the strengths of the Love numbers mainly come from the modes trapped within the reciprocal singular bound. On the other hand, if we fix the reciprocal singular bound and increase the thickness of the lithosphere, the strength of the Love numbers will quickly leak to the modes originally outside the reciprocal singular bound (Figs 1f and 3).

These two observations provide a basic and intuitive guide to the rest of the analysis.

3 THE ISOLATION FUNCTION

3.1 Definition

Consider an open-ended box contour C in the complex $z = x + iy$ plane (Fig. 4). Fixing all the dimensions of C except for

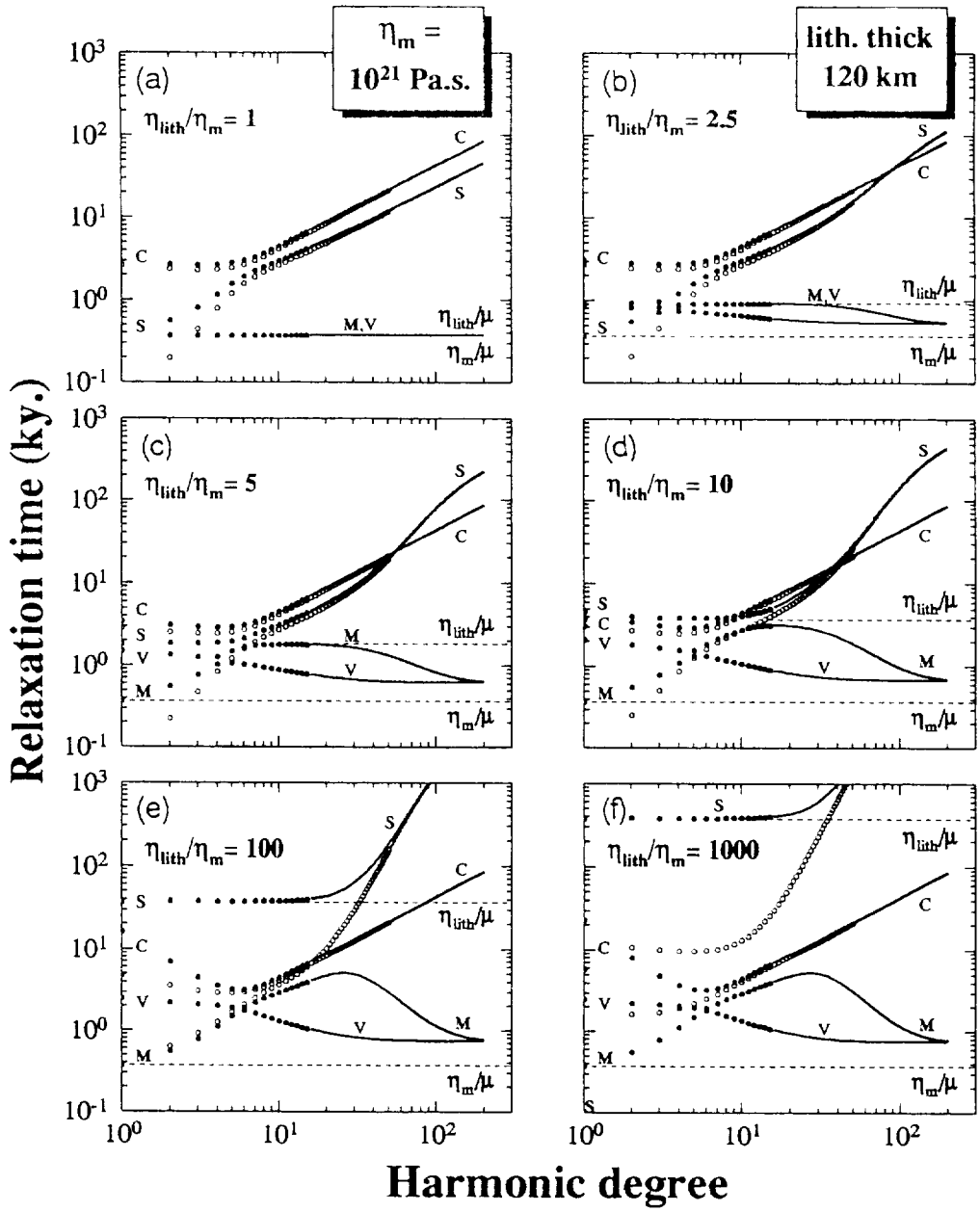

Figure 1. Relaxation times of the two-layer viscosity, otherwise uniform, mantle. The thickness of the lithosphere is fixed at 120 km, the mantle viscosity η_m is fixed at 10^{21} Pa s, and the lithospheric viscosity η_{lith} varies as indicated in each of the windows. Other necessary physical parameters needed for the calculations are listed in Fig. 7. The circles are for a Newtonian viscous mantle, and the dots are for a Maxwell viscoelastic mantle. The reciprocal singular bounds are marked by dashed lines (from Fang *et al.* in preparation).

the x coordinate of the open end, one can create a function of x by means of the contour C integral of a specific integrand $w(z)$. Next, we shrink the height ε of C, which is parallel to the imaginary axis, to zero in such a way that the real axis is always between the two sides of C (Fig. 4). We define the isolation function $I_w(x)$ as

$$I_w(x) = \lim_{\varepsilon \to 0} \frac{1}{2\pi i} \oint_{C(x)} w(z)\, dz, \qquad (x \le x_{fix}).$$

Except when mentioned otherwise, we assume that singularities of $w(z)$ are on the real axis and that poles are all of first order.

One can verify that, if $w(z)$ has one pole at x_0 within the interval (x, x_{fix}), the isolation function $I_w(x)$ is equal to the residue of the pole. In fact, as the height shrinks to zero, the contribution of the height on either side of a closed box contour to the integral will tend to zero; as a result, the closed box is equivalent to an open-ended box in the limit. As a demonstration, we examine the isolation function of the integrand

$$w(z) = \frac{1}{z - z_0},$$

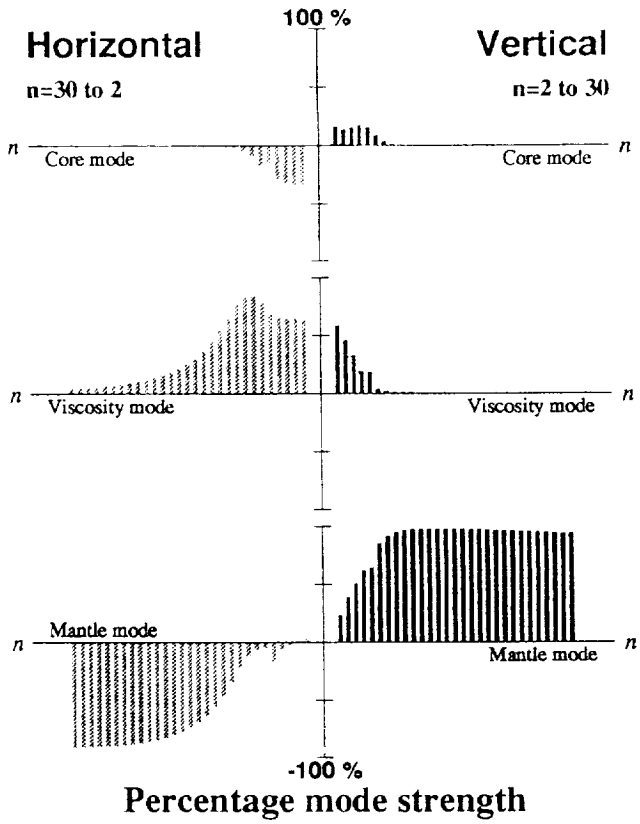

Figure 2. Percentage strength of the modes in the viscous part of the load Love numbers. The definition of the strength can be found in the text. The earth model use in the calculation is in Fig. 1(f). The S mode contribution is not plotted. The total contribution of the plotted C, V and M modes is nearly 100 per cent of the total strengths of the Love numbers, indicating that the S mode contribution is negligible.

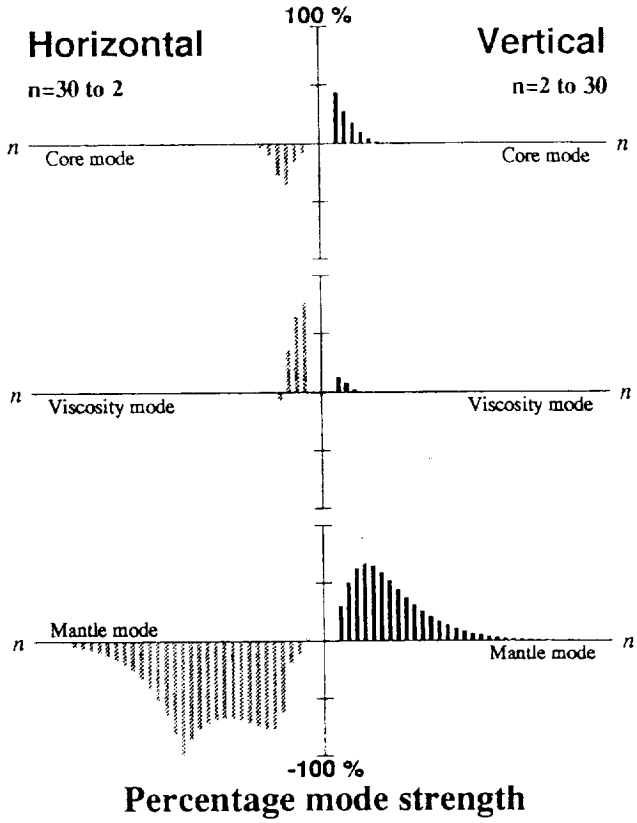

Figure 3. As Fig. 2, except that the thickness of the lithosphere is increased to 1000 km. The total contributions of the plotted C, V and M modes are significantly less than 100 per cent of the total strength of the Love numbers, especially at higher degrees. The deficiency of the total strengths is the contribution of the S modes.

where $z_0 = x_0$, $(x_0 \le x_{\text{fix}})$. One can easily obtain

$$I_w(x) = \lim_{\varepsilon \to 0} \frac{1}{2\pi i} \oint_C \frac{1}{z - z_0}\, dz = \lim_{\varepsilon \to 0} \frac{1}{\pi} \int_x^{x_{\text{fix}}} \frac{\varepsilon}{(x' - x_0)^2 + \varepsilon^2}\, dx'$$

$$= \begin{cases} 1 & x \le x_0, \\ 0 & x > x_0, \end{cases} \qquad x_{\text{fix}} > 0. \tag{10}$$

This is a step function, jumping in value at the pole z_0 of w. If there are several poles on the left side of x_{fix}, $I_w(x)$ will be a multistep function with the same number of jumps (falls) as of poles (Fig. 4). The amplitude of each relative jump (fall) is the residue of the pole. If there is a spectrum of 'continuous poles', or a branch cut, $I_w(x)$ will become a continuous function of x, as illustrated in Fig. 4. Note that eq. (10) indicates that the limit sign and integral sign in the isolation function are generally not interchangeable.

3.2 Continuous poles

The mechanism for causing the continuity of the isolation functions by branch cuts is well known (e.g. McLachlan 1955). But 'continuous poles' or a continuous distribution of non-isolated poles are not often seen in the literature. Thus, we need to formulate them here. Following an informal spirit, a continuous viscosity can be viewed as the limit of a sequence of multilayered viscosity models, with the number of layers

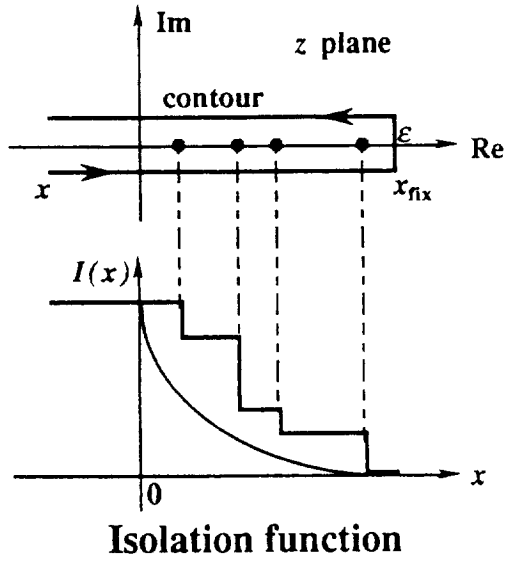

Figure 4. A picture demonstrating the open-ended box contour and the isolation function. ε is the height of the contour and is supposed to shrink to zero. No singularities, except the four poles represented by the four dots, are on the real axis between x and x_{fix}. The dashed line indicates that each pole corresponds to a step in the isolation function $I(x)$. The continuous curve illustrates what the isolation function looks like when branch cuts, or 'continuous poles', occur between x and x_{fix}.

tending to infinity. Without seeking mathematical generality, we can formulate 'continuous poles' as the limit of a sequence of finite poles.

Suppose there are M poles of the integrand $w(z)=f(z)e^{zt}$ within a bounded interval (x_0, x_{fix}). The isolation function with a constant parameter t is

$$I_w(x,t)=\sum_{j=1}^{M} r(x_j)e^{x_j t}H(x_j-x) \qquad (x_0<x_1<\cdots<x_M<x_{fix}),$$

where $r(x_j)$ is the residue of the pole at x_j, and H is the Heaviside function. Since (x_0, x_{fix}) is bounded, we will encounter cluster points in the sequence of poles as $M\to\infty$. If the number of cluster points is finite, we have a dense mode distribution only at these isolated cluster points. This is a peculiar situation where we find neither a discrete mode distribution nor a continuous spectrum of modes. To form a continuous spectrum of modes, the number of cluster points must be infinite. For simplicity, we assume that the poles are always nearly evenly distributed within (x_0, x_{fix}). This assumption is supported by the observations from the experiment with simple layered models (see Section 2). For a distribution with an infinite number of poles in a finite region, the residues of all the poles must tend to zero as $M\to\infty$, except for a finite number of them, otherwise $I_w(x,t)$ will tend to infinity, which is physically unacceptable. In mathematical terms, we have that

$$\lim_{M\to\infty} r(x_j)=0, \qquad \lim_{M\to\infty}(x_{j+1}-x_j)=0, \qquad j=1,2,3,\ldots \tag{11}$$

are true almost everywhere within (x_0, x_{fix}).

Using eq. (11), we can define the density of the residue $\xi(x_j)$ as

$$\xi(x_j)=\frac{r(x_j)}{(x_{j+1}-x_j)}.$$

Note that, at those exceptional points x_j where the residues have finite amplitude $\lim_{M\to\infty} r(x_j)\neq 0$, the density $\xi(x_j)$ is in the form of a Dirac delta function. So, generally, we have

$$I_w(x,t)=\lim_{M\to\infty}\sum_{k=1}^{M}\xi(x_j)e^{x_j t}H(x_j-x)(x_{j+1}-x_j)$$
$$=\int_x^{x_{fix}}\xi(x')e^{x't}\,dx'. \tag{12}$$

Relations (11) and (12) give the meaning to the frequently used term 'continuous spectrum of modes' in this specific situation. In particular, relations (11) simply state that the residue of almost every individual pole in the continuous spectrum is zero, while eq. (12) states that the zero-contribution poles as a whole may have a significant contribution to the isolation functions. The treatment introduced here is not limited to the first-order poles going continuous. The difference between first-order and higher-order poles only lies in the method of extracting the residues $r(x_j)$. For second- and higher-order poles, the residues r are also, in general, functions of time. In our formulation for the continuous spectrum of modes, the time variable can be considered as a constant. For a distribution of non-pole singularities, the formulation of a continuous spectrum of modes from 'continuous poles' may fail, but the isolation function as defined by a contour integral on the complex plane is still meaningful. In fact, we can use the isolation function, at least symbolically, to define a continuous spectrum of modes (see below).

3.3 The isolation function for Love numbers

The endpoints of the singular bound $[s_{min}, s_{max}]$ of a continuous viscosity model are

$$s_{min}=\min\left[-\frac{\mu}{\eta(r)}\right], \qquad s_{max}=\max\left[-\frac{\mu}{\eta(r)}\right].$$

For a continuous viscosity, every single point within $[s_{min}, s_{max}]$ corresponds to at least one singularity while for a two-layer viscosity, only the endpoints of the singular bound, s_{min} and s_{max}, correspond to singularities. However, distinguishing between the two types of singular bounds does not seem to be important, and we will not do so.

The Laplace inversion for the Love numbers in response to a Heaviside load history is

$$\tilde{w}_n(t)=\lim_{N\to\infty}\frac{1}{2\pi i}\int_{\sigma-iN}^{\sigma+iN}\tilde{w}_n(s)\frac{e^{st}-1}{s}\,ds, \qquad \sigma>0, \tag{13}$$

where $\tilde{w}_n$ represents either $\tilde{h}_n$ or $\tilde{l}_n$. Performing the usual trick in complex analysis, the integral (13) can be carried out, in the s plane, on the open-ended box contour (Fig. 5). Note that the contour in Fig. 5 excludes the origin $s=0$. The right end of the contour extends a little bit to the right of s_{max} by a small distance $\delta_1\geq 0$. We shrink the height of the contour the way we did before and reduce the complex expression (13) to a real expression

$$\tilde{w}_n(t)=\lim_{\varepsilon\to 0}\frac{1}{\pi}\int_{\omega_{min}}^{\omega_{max}}f_n(s)e^{-\omega t}\,d\omega$$
$$+\sum_j\frac{r_j}{s_j}(e^{s_j t}-1), \qquad (s=-\omega+i\varepsilon), \tag{14}$$

$$f_n(s)=\frac{\tilde{w}_n^r(-\omega\sin\varepsilon t-\varepsilon\cos\varepsilon t)+\tilde{w}_n^i(-\omega\cos\varepsilon t+\varepsilon\sin\varepsilon t)}{\varepsilon^2+\omega^2},$$

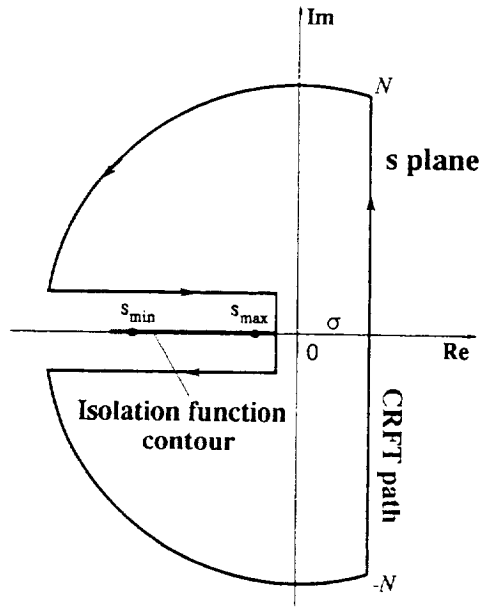

Figure 5. The contour for the Laplace inversion. The radius of the arcs will tend to infinity, and the height of the open-ended box shrinks to zero. The isolation function contour is shown as part of the shrunken open-ended box (the thick segment). As a comparison, the integral path used in the CRFT method (Fang & Hager 1994) is also indicated.

where $\tilde{w}_n^r$ and $\tilde{w}_n^i$ are the real part and imaginary parts of $\tilde{w}_n(s)$, respectively, the integral limits are $\omega_{\min} = -s_{\max} - \delta_1$, $\omega_{\max} = -s_{\min} + \delta_2$, $\delta_1, \delta_2 \geq 0$ and r_j, s_j are, respectively, the residual and location of the jth pole found outside the integral interval $(-\omega_{\max}, -\omega_{\min})$. In reaching eq. (14), we have used the property that the complex conjugate of the Laplace transform of a real function can be obtained by replacing the Laplace variable s with its conjugate. Eq. (14) can be interpreted as the complete eigen-expansion for the Love numbers with both a continuous spectrum and a discrete spectrum.

Again, the formulation of the integral term in (14) does not exclude the possibility of a number of modes with finite amplitudes sticking out among other 'continuous modes'. In this case, the density function $f_n(s)$ will tend to the Dirac delta function as $\varepsilon \to 0$. Another possibility is that there are branch cuts extending out of the singular bound. In this case we can use the quantities δ_1 or δ_2, or both, in case it is necessary, to extend the singular bound so as to include the branch cuts in the integral (14). If no branch cuts extend out of the singular bound, we can set δ_1 and δ_2 to small positive values to make sure that the endpoints of the singular bound are fully counted in a numerical evaluation of the integral (14). The variable ω represents the reciprocal relaxation time. It also conforms to the general sense of a function with a positive ascending argument. For simplicity, both $(-\omega_{\max}, -\omega_{\min})$ and $(\omega_{\min}, \omega_{\max})$ are referred to the same extending singular bound, as they indeed are.

The isolation functions for the Love numbers are defined on the extended singular bound. With a slight change of notation, we have

$$I_{\tilde{w}_n}(-\omega, t) = \lim_{\varepsilon \to 0} \frac{1}{\pi} \int_{\omega}^{\omega_{\max}} f_n(s') e^{-\omega' t} \, d\omega', \quad (\omega_{\min} \leq \omega \leq \omega_{\max}). \tag{15}$$

One question remains: how does the isolation function behave numerically? The key issue is whether a numerical integration of (15) can give a robust approximation to a step function. Fig. 6 shows the numerical result of the test integral (10). Since the numerical integration will blow up at the exact value $\varepsilon = 0$, the limit of ε is stopped at $\varepsilon = 0.002$. The integral spacing is chosen as 0.001, and the upper limit x_{fix} is fixed at 1. Fig. 6 clearly indicates that the isolation function is robust enough numerically to isolate the effects of modes.

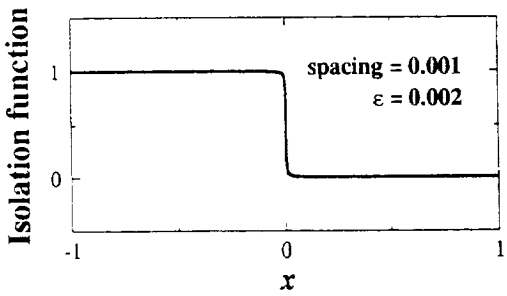

Figure 6. The numerical result of the isolation function for the integrand $1/z$. The uniform spacing for the numerical integration is chosen as 0.001, and the limits stopped at $\varepsilon = 0.002$.

4 RESULTS

4.1 Viscosity models

Four sets of viscosity models, A, B, C, and D, are used in this study (Fig. 7). The singular bounds $[s_{\min}, s_{\max}]$ for all of the viscosity models here are the same, with the endpoints

$$s_{\min} = -\frac{\mu}{\eta_0}, \qquad s_{\max} = -\frac{\mu}{53.7\eta_0}.$$

Obviously, the singular bound is not a sufficient measure to count for the contributions of various viscosity structures. We define the convexity of the viscosity models as illustrated by Fig. 7. The exact measure of convexity for a viscosity model $\eta(r)$ is

$$\begin{aligned} &\sup_{r_{\text{CMB}} \leq r \leq r_{670}} \left[\eta_{670} + \frac{\eta_{\text{CMB}} - \eta_{670}}{r_{\text{CMB}} - r_{670}} (r - r_{670}) - \eta(r) \right] \quad \text{for A}, \\ &\sup_{r_{670} \leq r \leq r_a} \left[\eta(r) - \eta_{670} + \frac{\eta_a - \eta_{670}}{r_a - r_{670}} (r - r_{670}) \right] \quad \text{for B}, \end{aligned} \tag{16}$$

where subscript a denotes the surface and other subscripts mark the depth. The definition (16) simply states that, within the same singular bound, a linear variation of viscosity always has zero convexity, the quadratic and exponential variation of viscosities always have negative convexities and a layered viscosity always has positive convexity. Note that the convexity for a layered viscosity is just the thickness of the layer (see Fig. 7).

4.2 Isolation functions for different viscosity models

The main results of this paper are the isolation functions (14) for the viscosity models in Fig. 7. We pick up harmonic degrees 4 and 15 for presentation here. The times are fixed at 1.2 kyr for degrees 4 and 4.2 kyr for degree 15. The horizontal isolation functions are in the form of

$$nI_{\tilde{l}_n}(-\omega, t).$$

Fig. 8 shows the isolation functions for lower mantle models A. Surprisingly, all the models in A have discrete mode structures within the singular bound. With the aid of Figs 1, 2, and 3, we can easily identify the M, V and C modes. The inclusion of the lithosphere brings about an additional viscosity discontinuity at the bottom of the lithosphere which will maintain two more modes. In total, the layered model in A has six modes. Because it is not a goal of this paper to identify modes, we simply term the modes other than M, V and C as X_1, X_2, and X_3, etc. For the continuous viscosity models in A, the minor modes are smoothed out, but the major modes remain. An inspection of the curves in Fig. 8 shows that the remaining major modes are also slightly smoothed, suggesting that the effect of the continuity of the lower mantle viscosity is not strong enough to split the discrete mode contribution into a continuous mode distribution. On the contrary, the continuous structure of the upper mantle viscosity has much stronger effects on splitting the discrete mode contribution into a continuous mode distribution. This feature can be seen in Figs 9 and 11. Furthermore, Figs 9, 10 and 11 quantitatively illustrate the situations where no discrete modes exist within the singular bound.

There have been a number of studies, some very recent, on

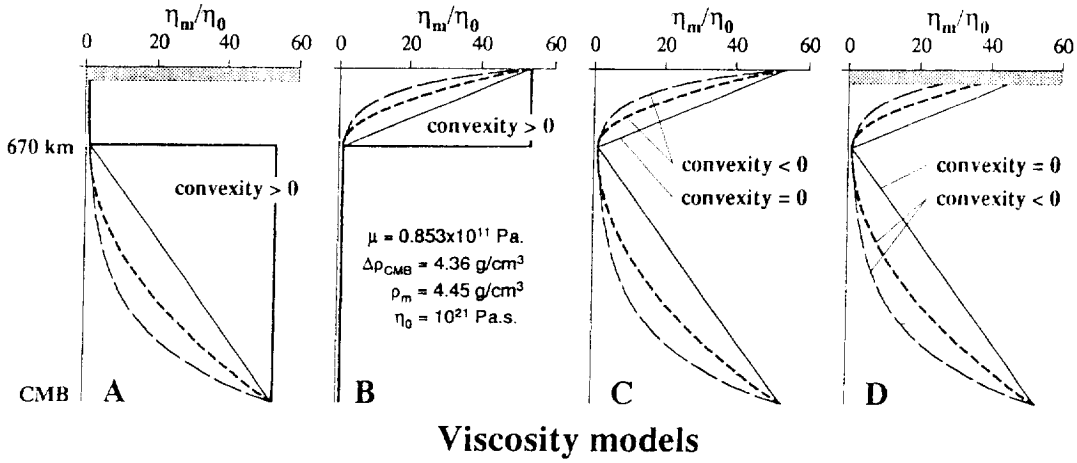

Figure 7. Viscosity models. Both model sets A and B contain a two-layer, an exponential, a quadratic and a linear model, while C and D do not have the two-layer model. Viscosity variations of A are within the lower mantle, starting with the value $\eta_m = \eta_0$ at 670 km depth to the value $\eta_m = 53.5\eta_0$ at the CMB. The upper mantle viscosity of A is uniform at the background viscosity η_0 except for a lithosphere. The lithosphere of A is modelled as a 120 km thick layer with the viscosity exponentially increasing from η_0 at the bottom to $10^6\eta_0$ on the surface (the shaded area). Viscosity models in B do not have a lithsophere and their variations are within the upper mantle, starting with the value $\eta_m = \eta_0$ at the 670 km depth and increasing to $\eta_m = 53.5\eta_0$ at the surface. The lower mantle viscosity of B is uniform at the background viscosity η_0. The model set C is a combination of A and B without the lithosphere, while D is a combination of A and B with the lithosphere.

the modal branches associated with simple layered viscosity models (e.g. Wu & Pelter 1982; Wolf 1985; James 1991; Amelung & Wolf 1994; Han & Wahr 1995; Mitrovica & Davis 1995). In all of these previous analyses, the M0 mode (equivalent to the M mode in this paper) is termed the fundamental branch of relaxation, and interpreted as arising from the density discontinuity at the outer surface of the Earth. This physical description of the M0 mode hardly fits the results of our analysis. Because the modal branches exchange elements, at lower degrees ($n \leq 6$), it is hard to decide, according to the 'movie' in Fig. 1, whether the M0 mode is related to the surface density contrast or to the viscosity contrast at the bottom of the lithosphere. At higher degrees ($n \geq 40$), it is clear, by comparing the viscous mode branches and viscoelastic branches in Figs 1(e) and (f), that the M0 and L0 modes (equivalent to the M and V modes, respectively, in this paper), belong to the pair of modes arising from the viscosity discontinuity at the bottom of the lithosphere. The mode arising from the surface density contrast joins the S branch at degrees $n \geq 40$. When the viscosity contrast at the bottom of the lithosphere is very large (Figs 1e and f), the S modes are way above the rest of the modal branches, and the contribution of the S modes to the time response is negligible (Fig. 2). Furthermore, if the M0 mode constitutes fundamental modes arising from the surface density discontinuity, it should stand out at all the harmonic degrees and display a certain kind of independence from the viscosity structure. Fig. 9 merely shows that the M mode at very low degree (e.g. degree 4) does show some independence from the viscosity models, suggesting that the M mode is due to the outer surface density contrast. However, at degree 15, the M mode is completely split into continuous mode distributions by stretching the viscosity contrast into continuous viscosity structures (Fig. 9). This feature hardly supports the interpretation that the M0 modes are due to the surface density contrast at degrees $n \geq 15$. Rather, it supports the assertion made above, that the M0 modes and L0 modes at higher degrees ($n \geq 15$) are the twin sisters arising from the viscosity contrast at the bottom of the lithosphere. The validity of this assertion may even apply to lower harmonic degrees.

A close inspection of the linear curve in Fig. 9 shows a number of blunt saw teeth in the vicinity of where the M mode arising from a layered structure is found. These saw teeth can be used to demonstrate how the M mode is split into a continuous distribution. A layered structure which has a positive convexity (the layered model in B in Fig. 7) generates the M mode. As we stretch the viscosity contrast into a continuous structure, the convexity of the model decreases. At zero convexity, we observe saw teeth in the vicinity of the former M mode, indicating that the single M mode is split into a number of small modes. As the convexity of the model decreases further, becoming negative, the saw teeth disappear, and the M mode is completely smoothed out. This phenomenon implies that, for certain classes of viscosity structures (e.g. monotonic functions within the same singular bound), the transition from a discrete mode distribution to a continuous mode distribution could be gradual and smooth.

For viscosity models having non-monotonic variation with depth, the situation is more complicated. A specific value in the singular bound $\omega(\omega_{min} < \omega < \omega_{max})$ corresponds to at least two singularities. For the combined models in C and D we have one singularity in the lower mantle and another in the upper mantle. The combined effect of the upper mantle continuous viscosity and lower mantle continuous viscosity provides smoother (Figs 10 and 11) isolation functions, and no saw-tooth structure is found with the viscosity of linear variation with depth. The smoothing effect is largely due to the upper mantle continuous viscosity structure (see analysis of Figs 8 and 9 above). The effect of the lower mantle continuous viscosity can be seen by comparing Figs 9 and 10. The pattern of gradual evolution in the isolation function from the single M mode structure to continuous mode distributions with a decrease of convexity disappears in Fig. 10, and a kind of irregular relationship in terms of their convexities shows up.

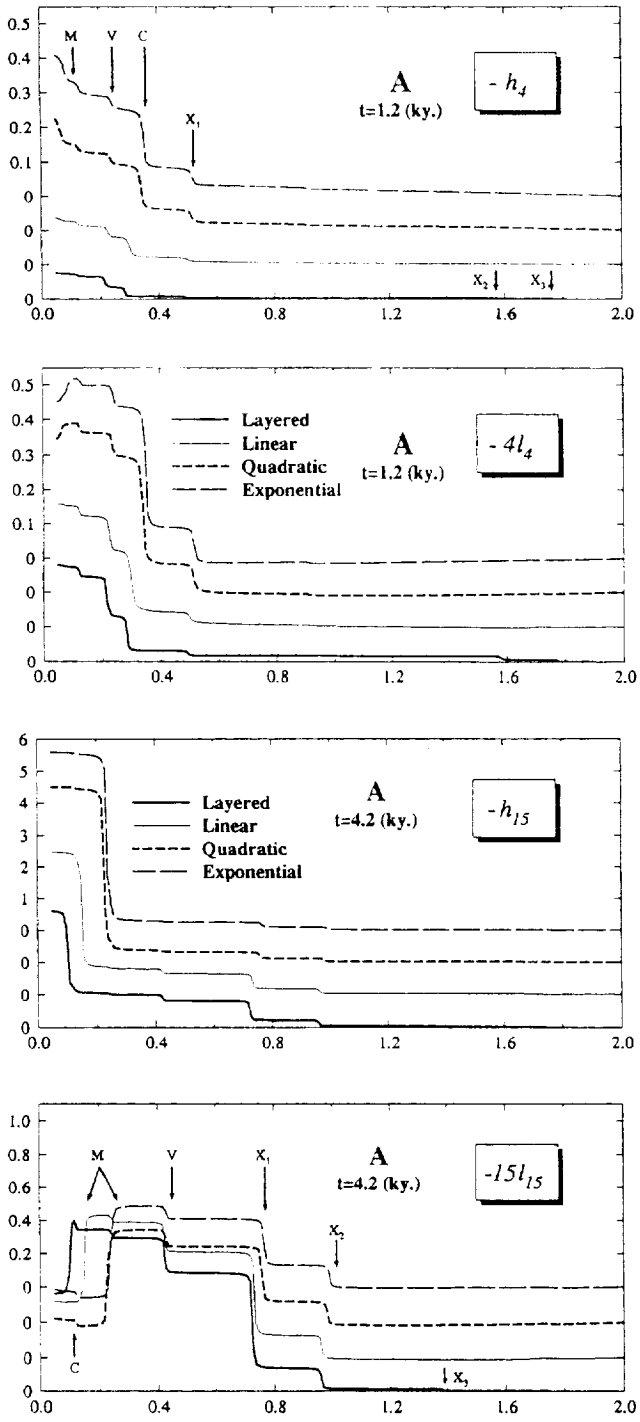

Figure 8. The isolation functions of the viscous part of the vertical and horizontal load Love numbers for viscosity models in A at harmonic degrees 4 and 15, respectively. To demonstrate the mode structures better, each curve is shifted consecutively by the amount of the annotation interval. Since the isolation functions all quickly tend to zero, one can easily identify the shift of each curve and calibrate it at the right zero level.

In general, all these figures (Figs 8 and 11) display a complicated relationship between a viscosity model and the spectra of the relaxation eigenfunctions associated with the model. This is in sharp contrast to the relationship between an elastic

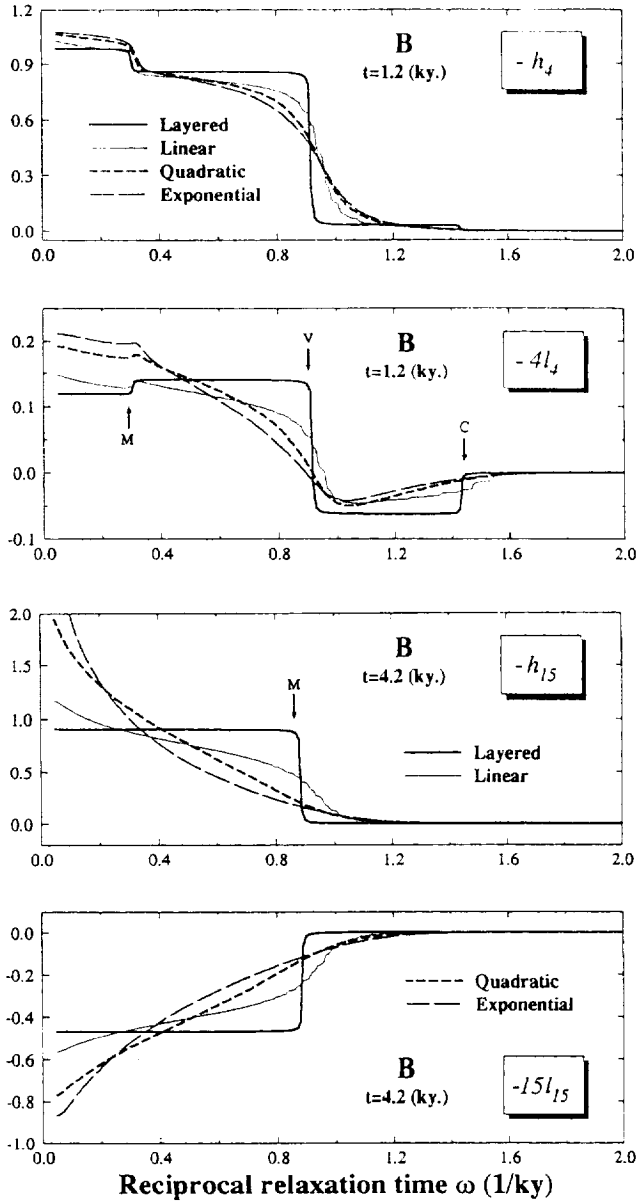

Figure 9. The same isolation functions as in Fig. 8, but for viscosity models in family B. The plots here are not shifted.

earth model and the elastic eigenfunctions (normal modes). The distribution of eigenfunctions for all elastic earth models is the same: grand modes ${}_0S_0, {}_0S_1 \cdots$ and overtones (e.g. Lapwood & Usami 1981). The eigenspace for all admissible elastic models can thus be easily established. However, here the distribution of relaxation eigenfunctions associated with a viscosity model depends upon the viscosity model itself in a non-linear way. This situation makes it much harder to establish the relaxation eigenspace for all admissible viscosity models.

The isolation functions (Figs 8 and 11) provide another means of revealing the differences between the vertical and horizontal responses. The difference can be observed with either the success (Fig. 8) or the failure of the discrete mode structure (Figs 9, 10 and 11). The essence of the difference, using the mode language, lies in the fact that major modes of

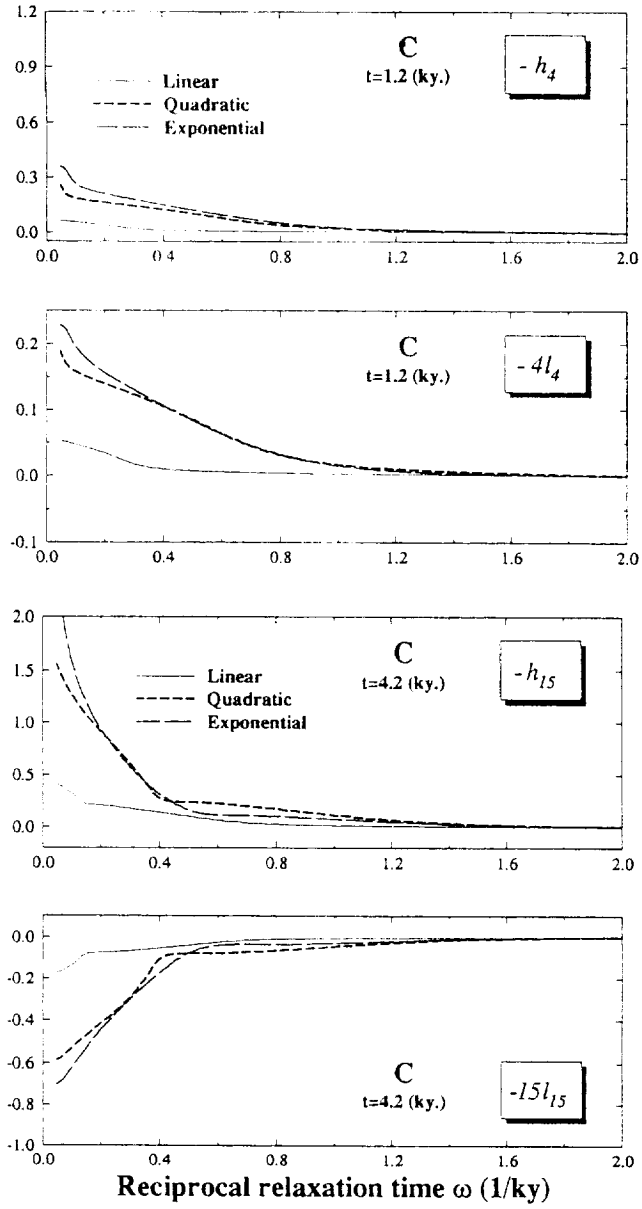

Figure 10. As Fig. 9, but for viscosity models in C.

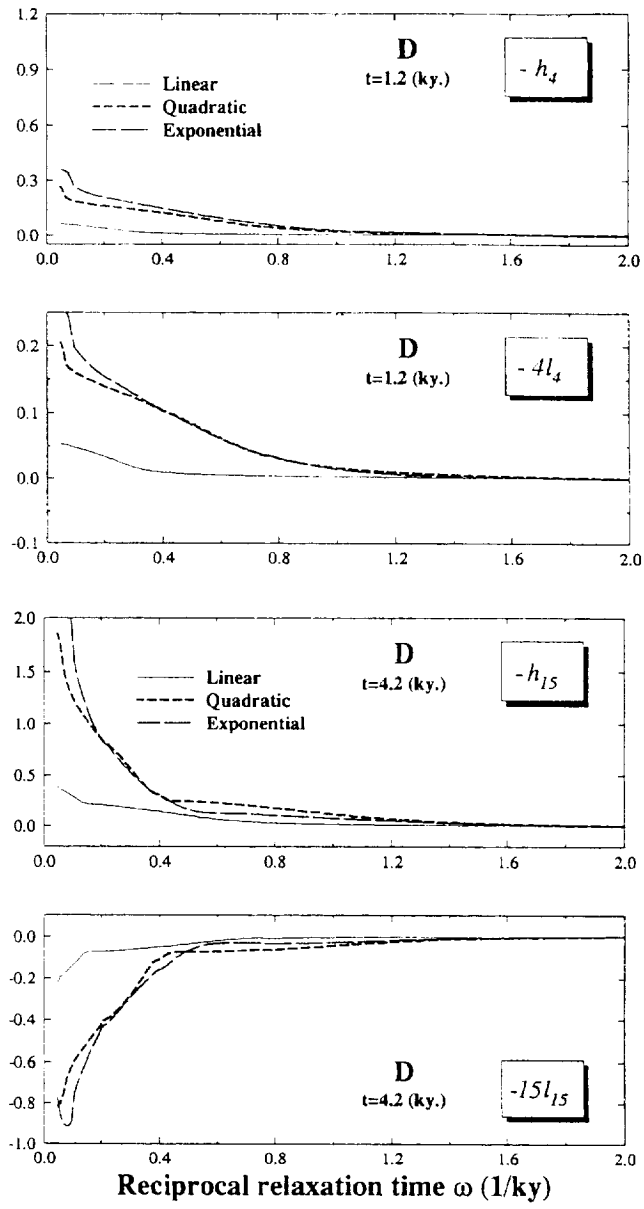

Figure 11. As Fig. 9, but for viscosity models in D.

the vertical response all have the same sign, while for the horizontal response, the V and M modes have opposite signs (Figs 2 and 3; Fang & Hager 1994; also see Mitrovica & Davis 1995).

4.3 Contributions from singular bounds

We have just seen in the last subsection both discrete mode and continuous mode structures within the singular bound. The following questions arise: (i) how much does a singular bound contribute to the total strength of Love numbers; (ii) when can a singular bound be dismissed? We look into the problem by examining the time variation of the Love numbers.

We calculate the time variation of the Love numbers, which, according to the inviscid fluid criterion (Wu & Peltier 1982), should be independent of viscosity models as $t \to \infty$. We then calculate the time variation of the singular bound contributions to the Love numbers. A comparison between the two independent calculations will provide a direct assessment of how much a singular bound contributes to the Love numbers at a given time. Since the horizontal motion is not sensitive to gravity, it is not directly related to the mechanism of isostasy. For this reason, we save the discussion of the horizontal motion for elsewhere, and concentrate on the vertical motion here. Figs 12 to 15 show the results for vertical responses. The time variations of the Love numbers are calculated using the CRFT method (Fang & Hager 1994). The singular bound contributions are calculated with the isolation function (15) by fixing ω at its lower limit, $\omega_{\min}$, and letting the time t vary.

A striking feature in Figs 12 to 15 is that the contributions of the singular bounds to the total Love numbers depend upon, and are even quite sensitive to, the convexities of the viscosity models (remember the singular bound for these viscosity models is the same). The characteristic relaxation

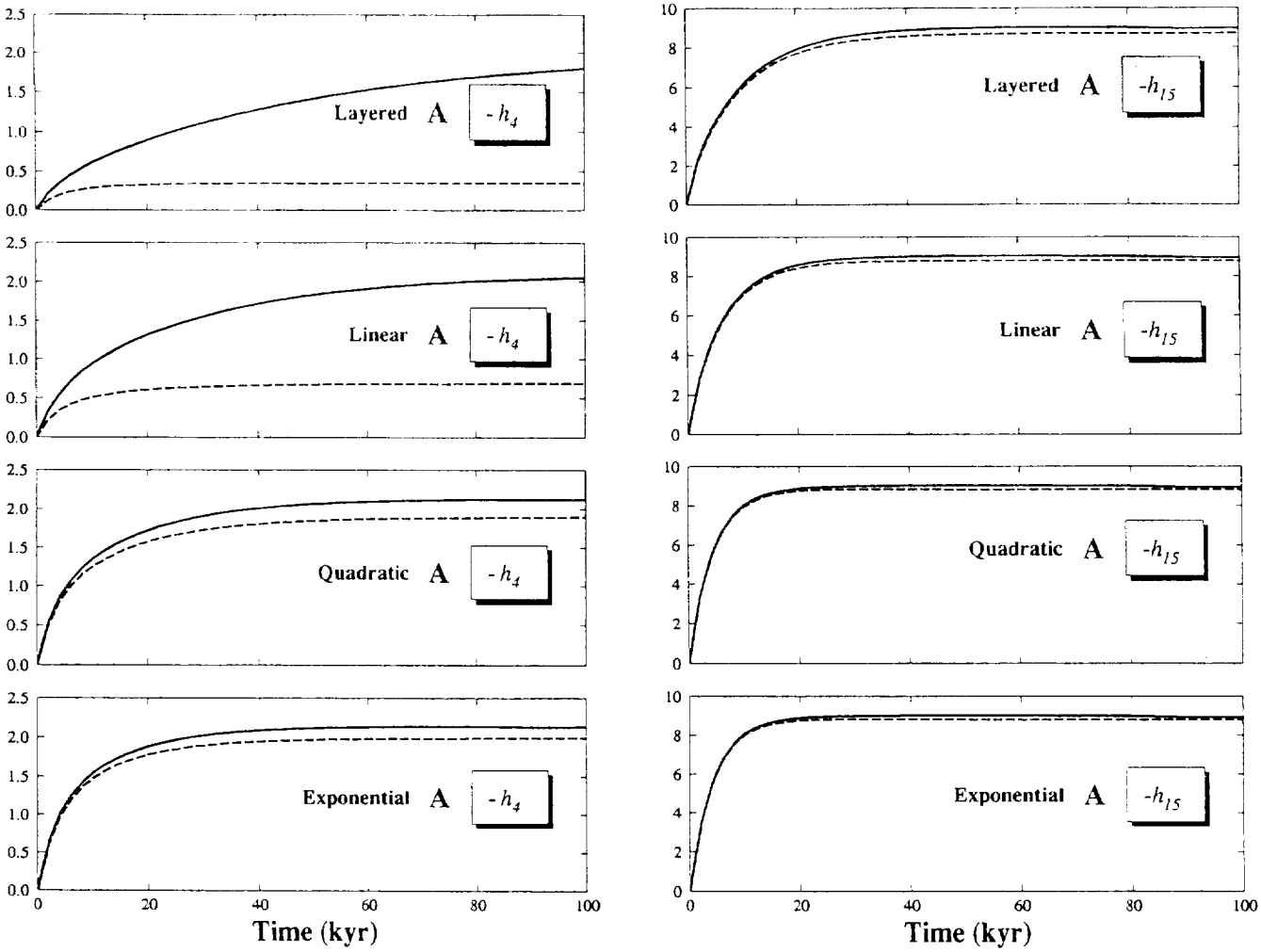

Figure 12. Time variations of the total Love number and the singular bound contributions for the viscosity models in family A. The total Love numbers are calculated using the complex-real Fourier transform (CRFT) method (solid line). The singular bound contributions are calculated with the isolation function (dashed lines).

time of a Maxwell rheology is η/μ, which measures the effect of viscous damping (resistance) of the dashpot element against the instantaneous elastic response of the spring element. The convexity of a viscosity model as a whole measures the relative importance of the viscosity effect among the models within the same singular bound and thus represents the relative degree of viscous damping. With the singular bound fixed, the larger the convexity, the heavier the viscous damping. As revealed in Figs 12 to 15, it takes a longer relaxation time in the case of heavier viscous damping for the total Love numbers to reach the final state of complete isostasy. The contribution of the singular bound to the total Love numbers, on the other hand, is smaller in the case of heavier viscous damping. For the exponential viscosity models, which have the smallest convexity, the singular bound contribution dominates the strengths of the total Love numbers. We have seen in the last subsection that there is effectively no fundamental modal branch arising from the outer surface density contrast and spanning the spectrum of all harmonic degrees for all viscosity models. Here, we further confirm that, for a certain class of viscosity models, the contribution from the fundamental modes, if they exist, is negligible.

The layered viscosity model in group B has an exact mode solution, as outlined in Section 2. It is equivalent to a uniform lithosphere of 670 km thickness overlying a uniform mantle. As seen in Fig. 13 (layered), the modes trapped within the singular bound, including the M modes, no longer dominate the total strength of the Love numbers with such an artificially thickened lithosphere. The same feature has been observed in Fig. 3. Fig. 13 clearly indicates that what we have observed in Fig. 3 is just a special case of the general situation where, with the singular bound fixed, heavier viscous damping results in less singular bound contribution to the Love numbers.

The relationship revealed in Figs 12 to 15 between the convexity of a viscosity model and the singular bound contribution to the Love numbers is very useful in evaluating the previous results and predicting the singularity effect on a new model. As an example, we see that the predicted effective viscosity, based on diffusion creep theory, is close to an exponential function (e.g. Ranalli 1991). For an estimate, we choose the viscosity near the D'' region to be $150\eta_0$, and the viscosity at 670 km depth to be η_0. These figures are quite conservative according to previous studies (e.g. Ranalli 1991). If the diffusion creep law dominates the lower mantle, we will

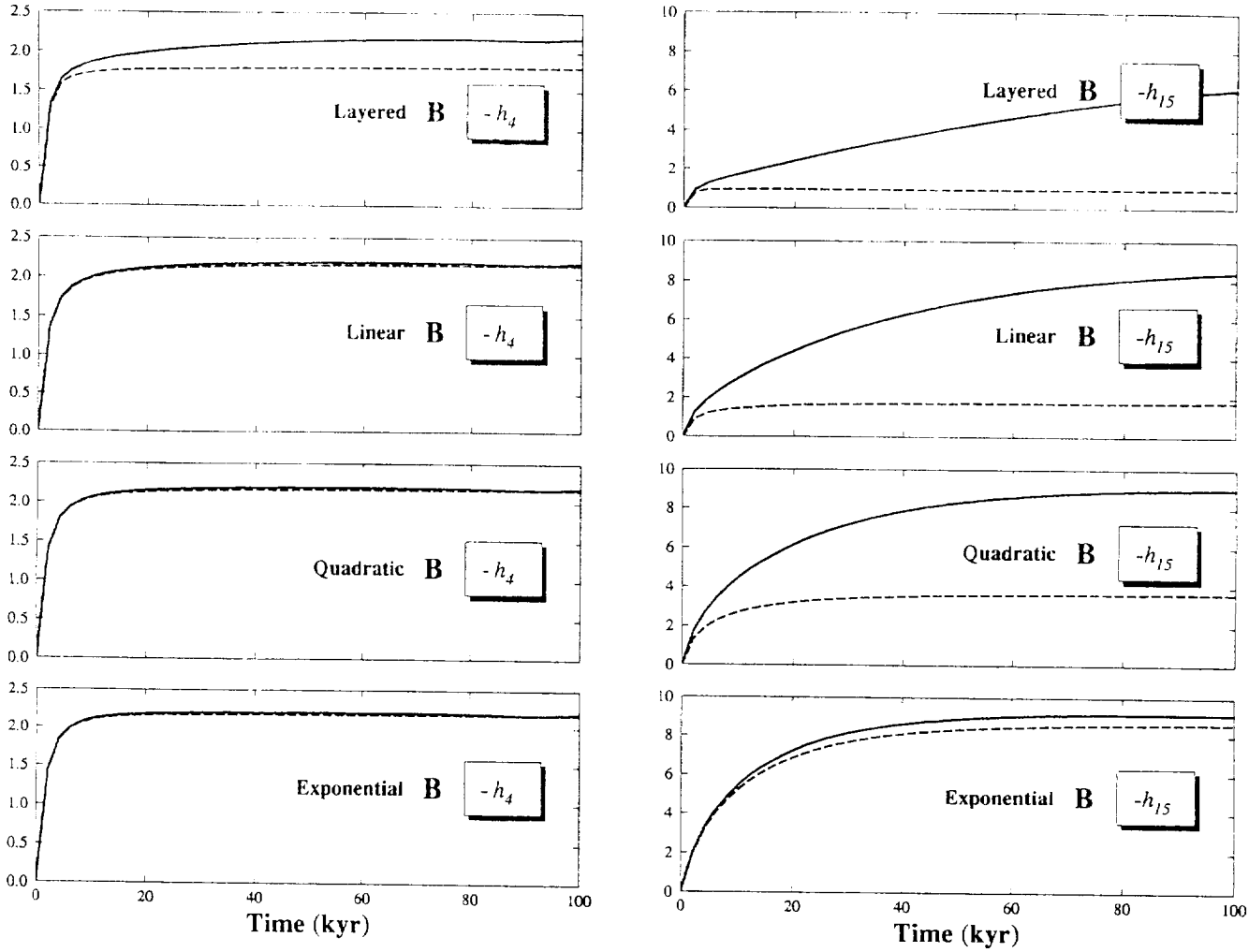

Figure 13. As Fig. 12, except for viscosity models in B.

have a 'realistic' viscoelastic parameter η/μ quite similar to that of the exponential model D in Fig. 7 [the 'realistic' shear modulus, e.g. Dziewonski & Anderson (1981), also has a modest increase with depth]. Hence, we can predict from Fig. 15 that a significant part of the total strength of the Love numbers will come from the singular bound. On the other hand, the viscoelastic parameters in Tushingham & Peltier's (1991) model have nearly zero convexity and a very small singular bound. We can reasonably anticipate that the contribution of the singular bound to the Love numbers for this model will be small. These two predictions are indeed correct (see Fang *et al.* in preparation).

A rule of thumb for spherical harmonic expansions in a wide range of problems is that the variation of upper mantle physical properties has little effect on the lower harmonic degree, while the variation of the lower mantle physical properties has little effect on the higher degrees. This rule of thumb also applies to our problem. As seen in Figs 12 and 13, the lower mantle viscosity variation has little impact on degree 15, while the upper mantle viscosity variation has little effect on degree 4. Interestingly, at degrees where the viscosity variations do not have much effect, the singular bound contributions become as large as even up to 95 per cent of the total strengths of the Love numbers. For the combined models C and D, in which the upper mantle viscosity and lower mantle viscosity vary simultaneously, all degrees are affected as expected (Figs 14 and 15). The lithosphere is a very shallow structure and therefore the C and D groups are nearly identical at degree 4 and show some difference at degree 15 (Figs 14 and 15).

5 CONCLUSION

We have designed and implemented an isolation function for the load Love numbers by manipulating the topology of the contours in the Laplace transform s plane. Using the isolation function, we are able to scan through the entire singularity distribution created by a radially inhomogeneous Maxwell viscoelastic structure, and to touch upon a number of unsolved problems associated with the singularities. We sum up, in the following, the major results of this investigation.

The discrete mode assumption for the Maxwell viscoelastic rheology is valid with finite layer viscoelastic parameter models (VEPMs). For VEPMs that are continuous functions of radius, the notion of discrete modes is only valid outside the singular bound. The general form of the dynamic response of a Maxwell viscoelastic earth contains a continuous spectrum of relaxation within the singular bound and a number of possible discrete relaxation modes outside the singular bound (eq. 14).

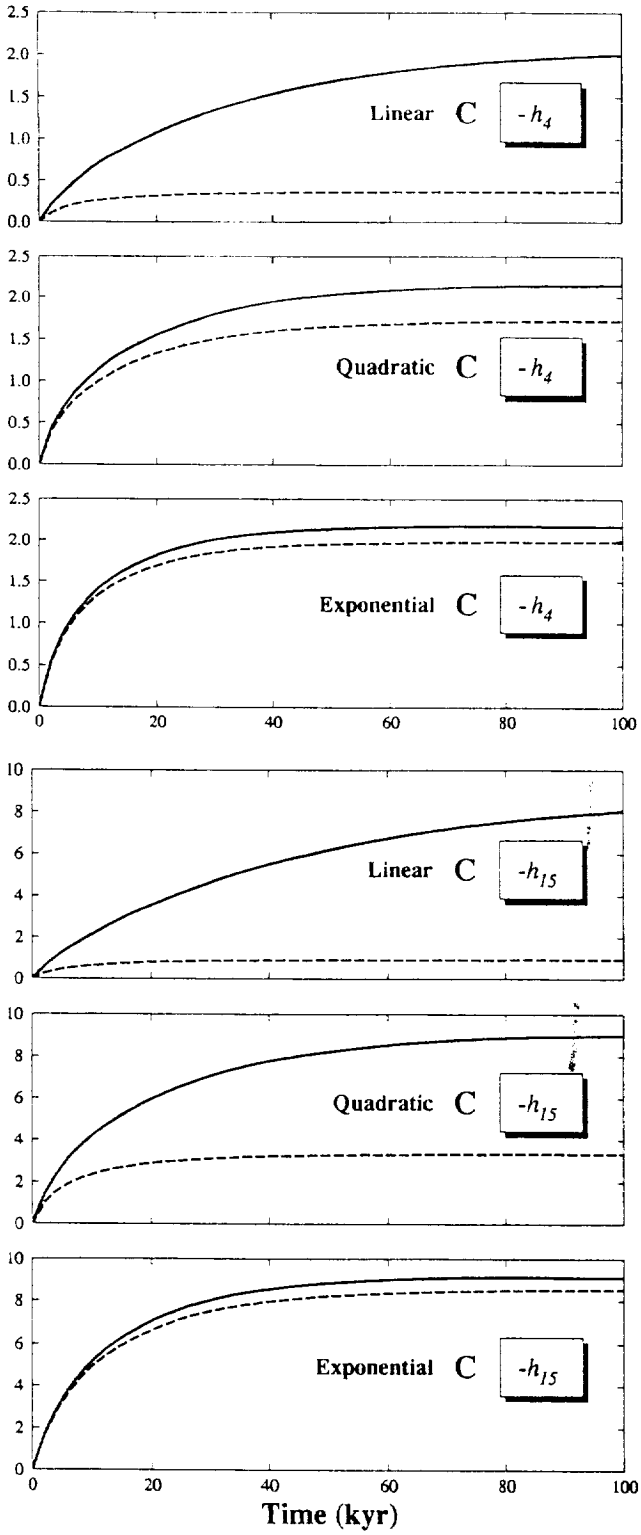

Figure 14. As Fig. 12, except for viscosity models in C.

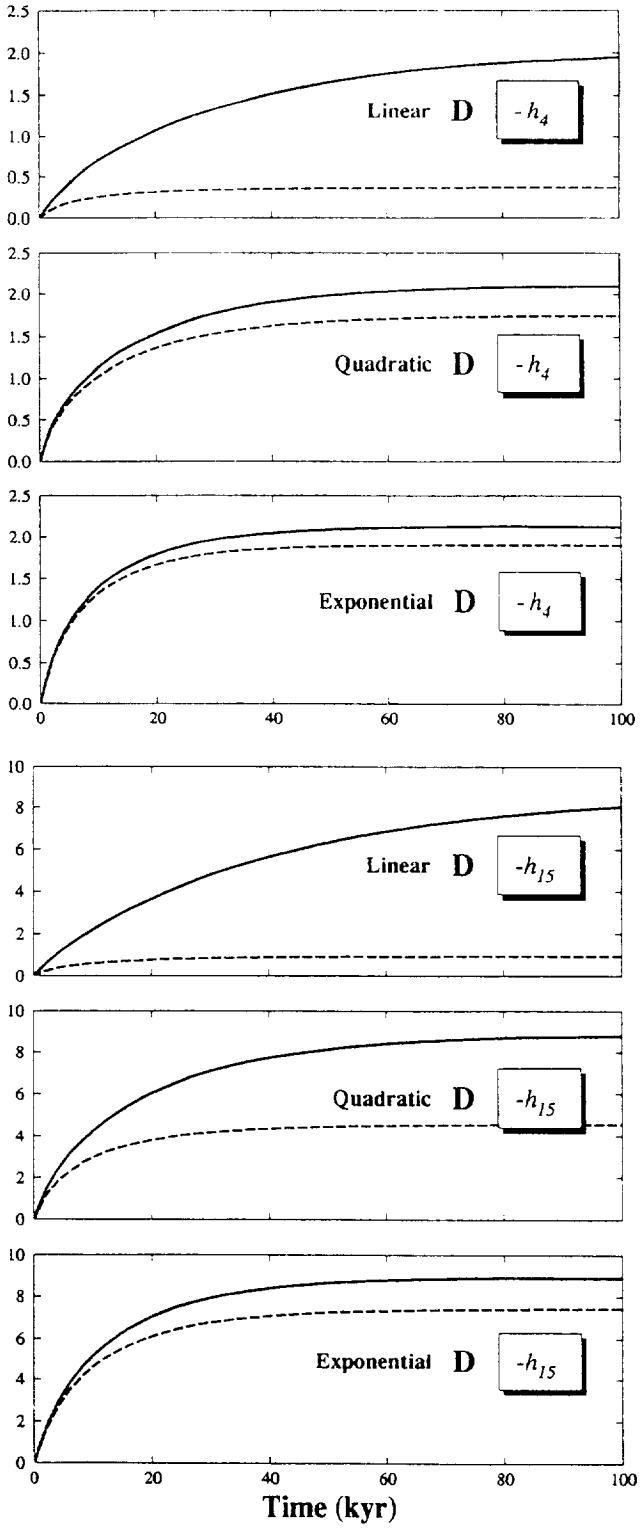

Figure 15. As Fig. 12, except for viscosity models in D.

The discrete mode-like response can remain within the singular bound provided that the upper mantle VEPM is homogeneous or layered or the lower mantle effect dominates the viscoelastic relaxation [see also Hanyk *et al.* (1995) for the latter case]. In these cases, a discrete mode approach can be adopted as an approximation. However, the search for modes within the singular bound has to follow the correct procedure given in the appendix of this paper. The continuity of the upper mantle VEPM plays a decisive role in splitting the discrete modes into continuous mode distributions within the singular bound. The inclusion of the lithosphere has little

impact against mode smearing by the continuous upper mantle VEPM.

The contribution of a fixed singular bound to the total strengths of the load Love numbers depends upon, and appears quite sensitive to, the convexity of the VEPM, which physically represents the relative degree of viscous damping among models within the same singular bound. For VEPMs of very positive convexity or heavier viscous damping, the load Love numbers are mainly determined outside the singular bound. For VEPMs of very negative convexity or lighter viscous damping, the major contribution to the load Love numbers is from within the singular bound. In particular, the theoretically predicted viscosity models have profiles of negative convexity, for example exponential functions of radius. We can be certain that singular bounds are indispensable in the studies of 'realistic' VEPM.

We have observed elsewhere (Fang & Hager 1994; Mitrovica & Davis 1995) that, for layered VEPMs, the major modes of the vertical response all have the same sign, but this is not true for the horizontal response. We found in this paper that such an observation extends to the 'continuous modes' within the singular bound (Fig. 9, model B, Fig. 10, model C). An indirect conjecture about such extension has been made by Fang & Hager (1994). The isolation function provides a direct and quantitative demonstration for the first time.

The modal branch M, often called 'fundamental', is not generated by the outer surface density contrast alone, as was widely believed in the past. At very low degrees, the M modes demonstrate characteristics of being generated by the outer surface density contrast. At higher degrees ($n \geq 15$), the M modes appear to be one of the twin modes generated by the viscosity contrast at the bottom of the lithosphere. When the viscosity discontinuity at the bottom of the lithosphere stretches into a continuous structure, the M modes split into a continuous mode distribution at higher harmonic degrees. The complexity of the physical causes of the M modal branch (also other modal branches) can be explained by the 'movie' in Fig. 1 which shows that modal branches undergo an exchange of elements during the evolution from low- to high-viscosity contrasts.

Finally, we discuss the validity of the simplifications made in this study. There are no new mathematical features involved in the extension of the incompressible uniform earth model used here to a 'realistic' earth model (e.g. PREM of Dziewonski & Anderson 1981). The major conclusions of this work can be extended to a 'realistic' earth model. The isolation function (15) is based on the Heaviside loading history. If we use a smoother loading history, the isolation function should be no more 'bumpy' than that of a Heaviside. Therefore, our conclusions can be extended to a 'realistic' loading history. Our results concerning the convexity of the VEPM do not include piecewise continuous structures and oscillating structures of the VEPM. In these cases, the definition of convexity of a VEPM profile becomes meaningless. However, we can evaluate the degree of viscous damping by looking at the average of the viscosity structure. We believe that what we have found here, namely the heavier the damping, the less the singular bound contribution to the Love numbers, is true in general.

ACKNOWLEDGMENTS

We thank Drs Mitrovica, Peltier and Wahr for careful reviews and constructive suggestions. This study was supported by the Climate and Global Change Program of the National Oceanic and Atmospheric Administration (NOAA), grant NA24 GP0023, and by NASA DOSE grant NAG5-1911.

REFERENCES

Alterman, Z.S., Jarosh, H. & Pekeris, C.L., 1959. Oscillation of the Earth, *Proc. R. Soc. Lond.*, A, **252**, 80–95.

Amelung, F. & Wolf, D., 1994. Viscoelastic perturbation of the earth: significance of the incremental gravitational force in models of glacial isostasy, *Geophys. J. Int.*, **117**, 864–879.

Babister, A.W., 1967, *Transcendental Functions Satisfying Nonhomogeneous Linear Differential Equations*, Macmillan, New York.

Christensen, R.M., 1971. *Theory of Viscoelasticity*, Acad. Press, New York, NY.

Colombo, S., 1983. *Holomorphic functions of one variable*, Gordon & Breach, New York, NY.

Dziewonski, A.M. & Anderson, A., 1981. Preliminary reference Earth model, *Phys. Earth planet. Inter.*, **25**, 297–356.

Fang, M. & Hager, B.H., 1994. A singularity free approach to post glacial rebound calculations, *Geophys. Res. Lett.*, **21**, No. 19, 2131–2134.

Farrell, W.E., 1972. Deformation of the earth by surface loads, *Rev. Geophys. Space Phys.*, **10**, 761–797.

Han, D. & Wahr, J., 1995. The viscoelastic relaxation of a realistically stratified earth and a further analysis of post-glacial rebound, *Geophys. J. Int.*, **120**, 287–311.

Hanyk, L., Moser, J., Yuen, D.A. & Matyska, C., 1995. Time-domain approach for the transient reponses in stratified viscoelastic earth models, *Geophys. Res. Lett.*, **22**, 1285–1288.

James, T.S., 1991. Post glacial deformation, *Phd thesis*, Princeton University, New Jersey.

Lapwood, E.R. & Usami, T., 1981. *Free Oscillation of the Earth*, Cambridge Univ. Press, Cambridge.

McLachlan, N.W., 1955. *Complex Variable Theory and Transform Calculus*, Cambridge Univ. Press, Cambridge.

Mitrovica, J. & Davis, J.L., 1995. Some comments on the 3-D impulse response of a Maxwell viscoelastic earth, *Geophys. J. Int.*, **120**, 227–234.

Mitrovica, J. & Peltier, W.R., 1992. A comparison of methods for the inversion of viscoelastic relaxation, *Geophys. J. Int.*, **108**, 410–414.

Nakada, M. & Lambeck K., 1987. Glacial rebound and relative sea-level variations: a new appraisal, *Geophys. J. R. astr. Soc.*, **90**, 171–224.

Nakada, M. & Lambeck, K., 1989. Late Pleistocene and Holocene seal-level change in the Australian region and mantle rheology, *Geophys. J. R. astr. Soc.*, **96**, 497–517.

Peltier, W.R., 1974. The impulse response of a Maxwell Earth, *Rev. Geophys. Space Phys.*, **12**, 649–669.

Peltier, W.R., 1985. The LAGEOS constraint of deep mantle viscosity: results from new normal mode method for the inverse of viscoelastic relaxation spectra, *J. geophys. Res.*, **90**, 9411–9421.

Ranalli, G., 1991. The microphysical approach to mantle rheology, in *Glacial Isostasy, Sea-level, and Mantle Rheology*, NATO ASI Series Vol. 334, pp. 343–378, eds Sabadini, R., Lambeck, K. & Boschi, E., Kluwer, Dordrecht.

Richards, M. & Hager, B.H., 1984. Geoid anomalies in a dynamic Earth, *J. geophys. Res.*, **89**, 5987–6002.

Takeuchi, H. & Satio, M., 1972. Seismic surface waves, in *The Method in Computational Physics*, Vol. 11, pp. 217–295, eds Bolt, B.A. *et al.*, Acad. Press, New York.

Tushingham, A.M. & Peltier, W.R., 1991. ICE-3G: a new global model of late Pleistocene deglaciation based upon geophysical predictions of post glacial relative sea change, *J. geophys. Res.*, **96**, 4497–4523.

Weertman, J., 1978. Creep laws for the mantle of the earth, *Phil. Trans. R. Soc. Lond.*, A, **288**, 9–26.

Wolf, D., 1985. Dynamics of the continental lithospere, *PhD thesis*, University of Toronto, Toronto, Canada.

Wolf, D., 1994. Lamé problem of gravitational viscoelasticity: the isothermal, incompressible planet, *Geophys. J. Int.*, **116**, 321–348.

Wu, P. & Peltier, W.R., 1982. Viscous gravitational relaxation, *Geophys. J. R. astr. Soc.*, **70**, 435–485.

Wu, J. & Yuen, D.A., 1991. Post-glacial relaxation of a viscously stratified compressible mantle, *Geophys. J. Int.*, **104**, 331–349.

APPENDIX

The key to the correct procedure of mode searching within a singular bond is to provide initial values near the singularity point r_0. This requires an approximate solution of the basic eq. (1) expanded about r_0. Applying the $\nabla \times$ operator to eq. (1) and substituting the harmonic expansion of the variables into (1) and (2) we obtain

$$\frac{d^4U_n}{dr^4} + q_3(r,s)\frac{d^3U_n}{dr^3} + q_2(r,s)\frac{d^2U_n}{dr^2} + q_1(r,s)\frac{dU_n}{dr} + q_0(r,s)U_n = 0, \tag{A1}$$

$$\begin{cases} q_0 = \dfrac{(n-1)n(n+1)(n+2)}{r^4} + \dfrac{(n-1)(n+2)}{r^2E}\dfrac{d^2E}{dr^2}, \\ q_1 = -\dfrac{4n(n+1)}{r^3} + \dfrac{6-2n(n+1)}{r^2E}\dfrac{dE}{dr} + \dfrac{2}{rE}\dfrac{d^2E}{dr^2}, \\ q_2 = -\dfrac{2(n+3)(n-2)}{r^2} + \dfrac{10}{rE}\dfrac{dE}{dr} + \dfrac{1}{E}\dfrac{d^2E}{dr^2}, \\ q_3 = \dfrac{8}{r} + \dfrac{2}{E}\dfrac{dE}{dr}, \end{cases} \tag{A2}$$

where for Maxwell rheology the coefficient E can be written as

$$E = \frac{s\mu\eta(r)}{\mu + s\eta(r)}. \tag{A3}$$

Since the solution of (A1) itself is a meaningful subject and has not been tried before, in this appendix we first derive the power series solution of (A1) expanded about r_0. The correct procedure for mode searching within the singular bound will be outlined afterwards. Here we only consider a Maxwell rheology. The other two rheologies, Newtonian flow and elasticity, do not suffer from the non-zero singularity point r_0, and can be treated in a more complete fashion than we do here (e.g. Wu & Yuen 1991).

Consider the solution of (A1) within the mantle $r_{CMB} \le r \le r_a$. The only possible singularities of q_i $(i = 0, 1, 2, 3)$ in the mantle region are at those r_0 values satisfying

$$\mu + s\eta(r_0) = 0, \qquad (r_{CMB} \le r_0 \le r_a). \tag{A4}$$

It is easy to prove from eqs (A2), (A3) and (A4) that the following functions, $(r-r_0)^{4-k}q_k$ $(k = 1, 2, 3, 4)$, are all regular at r_0. Hence, we have the Taylor expansions

$$\begin{cases} (r-r_0)^4 q_0 = \sum_{k=0}^{\infty} a_k (r-r_0)^k, \\ (r-r_0)^3 q_1 = \sum_{k=0}^{\infty} b_k (r-r_0)^k, \\ (r-r_0)^2 q_2 = \sum_{k=0}^{\infty} c_k (r-r_0)^k, \\ (r-r_0) q_3 = \sum_{k=0}^{\infty} d_k (r-r_0)^k. \end{cases} \tag{A5}$$

The derivation of the coefficients a_k, b_k, c_k, d_k is very messy for large k. This proves to be the major problem for high-order approximation. However, it is not so difficult to derive the first few terms. The crucial terms are the zero-order coefficient a_0, b_0, c_0 and d_0. They can be evaluated by the following limits:

$$\begin{aligned} a_0 &= \frac{(n-1)(n+2)}{r_0^2}\lim_{r\to r_0}\left[(r-r_0)^4\frac{d^2E}{Edr^2}\right], \\ b_0 &= \frac{6-2n(n+1)}{r_0^2}\lim_{r\to r_0}\left[(r-r_0)^3\frac{dE}{Edr}\right] \\ &\quad + \frac{2}{r_0}\lim_{r\to r_0}\left[(r-r_0)^3\frac{d^2E}{Edr^2}\right], \\ c_0 &= \frac{10}{r_2}\lim_{r\to r_0}\left[(r-r_0)^2\frac{dE}{Edr}\right] + \lim_{r\to r_0}\left[(r-r_0)^2\frac{d^2E}{Edr^2}\right], \\ d_0 &= 2\lim_{r\to r_0}\left[(r-r_0)\frac{dE}{Edr}\right]. \end{aligned} \tag{A6}$$

Note that

$$\frac{dE}{Edr} = \frac{\mu}{(\mu+s\eta)\eta}\frac{d\eta}{dr}, \tag{A7}$$

$$\frac{d^2E}{Edr^2} = \frac{\mu}{(\mu+s\eta)\eta}\frac{d^2\eta}{dr^2} - \frac{2\mu s}{(\mu+s\eta)^2\eta}\left(\frac{d\eta}{dr}\right)^2, \tag{A8}$$

$$\lim_{r\to r_0}\frac{r-r_0}{\mu+s\eta} = \frac{1}{s}\left(\frac{d\eta}{dr}\right)^{-1}. \tag{A9}$$

Substituting eqs (A7), (A8) and (A9) into (A6) and making use of the singularity point eq. (A4), we obtain

$$a_0 = b_0 = 0, \qquad c_0 = -d_0 = 2. \tag{A10}$$

The general solution of (16) expanded at r_0 can be written as

$$U_n(r,s) = [r - r_0(s)]^{\lambda}\sum_{k=0}^{\infty} w_k(s)[r-r_0(s)]^k, \tag{A11}$$

where λ is the index for avoiding branch point. The parameter s is kept constant in seeking U_n as a function of r. It will be dropped for simplicity. Substituting eqs (A6) and (A11) into (A1), which is already multiplied by $(r-r_0)^4$, we obtain the indicial equation and recursive relation for the unknown coefficients w_k:

$$\begin{aligned} &\lambda(\lambda-1)(\lambda-2)(\lambda-3) + d_0\lambda(\lambda-1)(\lambda-2) \\ &\quad + c_0\lambda(\lambda-1) + b_0\lambda + a_0 = 0, \end{aligned} \tag{A12}$$

$$w_k f_0(\lambda+k) + \sum_{j=1}^{k} w_{k-j} f_k(\lambda+k-j) = 0, \qquad k = 1, 2, 3, \ldots,$$

$$\begin{aligned} f_0(\lambda) &= (\lambda-\lambda_1)(\lambda-\lambda_2)(\lambda-\lambda_3)(\lambda-\lambda_4), \\ f_k(\lambda) &= d_k\lambda(\lambda-1)(\lambda-2) + c_k\lambda(\lambda-1) + b_k\lambda + a_k, \end{aligned} \tag{A13}$$

where $\lambda_1, \lambda_2, \lambda_3$ and λ_4 are the four roots of the indicial eq. (A12). Using eq. (A10), we have

$$\lambda_1 = 4, \qquad \lambda_2 = 3, \qquad \lambda_3 = 1, \qquad \lambda_4 = 0. \tag{A14}$$

Substituting λ_1 into eq. (A13), we obtain the coefficients of the first independent solution with an arbitrary constant w_0 to be determined. Since all the roots of eq. (A14) are integers, substitutions of the rest of the roots into (A13) will not lead to

independent solutions. In this case, the Frobenius technique (see Babister 1967) must be invoked for the remaining three independent solutions. After the Frobenius operation, we complete the four independent solutions for (A1):

$$
\begin{aligned}
U_n^{(1)} &= \sum_{k=0}^{\infty} w_k (r-r_0)^{k+4}, \\
U_n^{(2)} &= \sum_{k=0}^{\infty} \left[\frac{\partial w_k}{\partial \lambda} + w_k \ln(r-r_0) \right] \Bigg|_{\lambda=3} (r-r_0)^{k+3}, \\
U_n^{(3)} &= \sum_{k=0}^{\infty} \left[\frac{\partial^2 w_k}{\partial \lambda^2} + 2\frac{\partial w_k}{\partial \lambda} \ln(r-r_0) \right. \\
&\quad \left. + w_k \ln^2(r-r_0) \right] \Bigg|_{\lambda=1} (r-r_0)^{k+1}, \\
U_n^{(4)} &= \sum_{k=0}^{\infty} \left[\frac{\partial^3 w_k}{\partial \lambda^3} + 3\frac{\partial^2 w_k}{\partial \lambda^2} \ln(r-r_0) + 3\frac{\partial w_k}{\partial \lambda} \ln^2(r-r_0) \right. \\
&\quad \left. + w_k \ln^3(r-r_0) \right] \Bigg|_{\lambda=0} (r-r_0)^k,
\end{aligned}
\tag{A15}
$$

where

$$
w_0 = \begin{cases} w_0 & (\text{in } U_n^{(1)}), \\ w_0'(\lambda-3) & (\text{in } U_n^{(2)}), \\ w_0''(\lambda-1)^2 & (\text{in } U_n^{(3)}), \\ w_0''' \lambda^3 & (\text{in } U_n^{(4)}). \end{cases}
$$

w_0, w_0', w'' and w_0''' are integral constants to be determined. With the vertical component U_n known, the horizontal component V_n can be derived through the continuity eq. (2), which gives

$$
V_n = \frac{1}{n(n+1)} \left(r\frac{dU_n}{dr} + 2U_n \right). \tag{A16}
$$

The rest of the derivation is straightforward and is thus omitted here.

The correct procedure to deal with the singularities using the propagation technique in search of modes is to terminate the propagation of eq. (5) from the centre somewhere below the singularity point r_0, and then re-initiate two sets of propagation starting at r_0. One of the propagations goes all the way up to the surface, and the other goes down to where the original propagation was terminated. The first few terms of the solution (A15) and (A16) can provide the initial values for the latter two propagations. An additional boundary is formed at the terminated radius. However, the downward propagation just brings an additional set of integral constants for that boundary. Hence, the solution of (5) at the surface can be uniquely determined. For problems with more than one singularity radius, such as the viscosity models C and D in Fig. 7, we can proceed following the same principle, that is to derive the expansion (A15) and (A16) at each singularity point, and create a cut-off boundary between each adjacent pair of singularity points.